Materials Characterization 223 (2025) 114915

Contents lists available at ScienceDirect

Materials Characterization

journal homepage: www.elsevier.com/locate/matchar

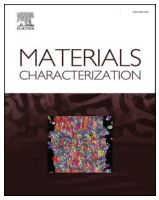

Identification and accurate characterisation of the metastable Co_{FCC} phase in WC–Co cemented carbides

Haoruo Zhou [a,b], Hansheng Chen [a,b], Christoph Czettl [c], Thomas Weirather [c], Julia Pachlhofer [c], Pauline Mueller [c], Tamara Teppernegg [c], Ralph Useldinger [d], Sophie Primig [e], Simon P. Ringer [a,b,*]

[a] School of Aerospace, Mechanical and Mechatronic Engineering, The University of Sydney, Sydney, NSW 2006, Australia
[b] Australian Centre for Microscopy and Microanalysis, The University of Sydney, Sydney, NSW 2006, Australia
[c] R&D Carbide and Coating, CERATIZIT Austria GmbH, Metallwerk-Plansee-Straße 71, AT-6600 Reutte, Austria
[d] CERATIZIT Luxembourg S. à r.l., 101 Route de Holzem, 8232 Mamer, Luxembourg
[e] School of Materials Science & Engineering, UNSW, Sydney, NSW 2052, Australia

ARTICLE INFO

Keywords:
Co martensitic phase transformation
Cemented carbides
Metallographic preparation workflow

ABSTRACT

Composed of hard tungsten carbide (WC) particles and a soft cobalt (Co) matrix, WC–Co cemented carbides exhibit significant differences in the material removal rates of these phases during metallographic preparation. This disparity, combined with the susceptibility of the soft Co phase to deformation-induced martensitic phase transformation from its face-centered cubic (Co_{FCC}) to hexagonal close-packed (Co_{HCP}) structure, poses substantial challenges for microstructural characterisation. The resulting ambiguity complicates the identification of the pristine Co phase and raises concerns about the presence of preparation-induced artefacts. In this study, we present a detailed comparative analysis aimed at minimizing ambiguities in the characterisation of the pristine Co phases in a series of WC–Co cemented carbides. We quantitatively report on the controllability of various preparation parameters under multiple conditions, for plane-polished cross-sections used in (e.g.) EBSD analysis and for thin-sections such as used in (e.g.) TEM analysis. We report on the interplay between material removal and the deformation-induced martensitic Co_{FCC}–Co_{HCP} phase transformation during metallographic preparation, identifying "GO" and "NO GO" regimes for the unequivocal identification of the pristine Co phase in WC–Co cemented carbides. The optimal metallographic preparation method for the "GO" regime involves an Ar^+ ion polishing energy density of ~10 MJ/m^2 and a duration of ~80 min. This work establishes a robust workflow for accurately determining the pristine Co phase, providing a pivotal aspect for the characterisation of microstructure–property relationships in WC–Co cemented carbides.

1. Introduction

As suitable materials for high-performance cutting tools, tungsten carbide–cobalt (WC–Co) cemented carbides possess an outstanding combination of hardness and fracture toughness due to the hard WC particles and a soft Co matrix [1–3]. Such mechanical properties rely on multiple microstructural features, such as the WC particle size and distribution [4], the frequency and types of the WC/WC grain boundaries and WC/Co phase boundaries [5,6], as well as the Co face-centred cubic (Co_{FCC})/Co hexagonal close-packed (Co_{HCP}) ratio [7,8].

So far, achieving accurate characterisation of the Co_{FCC}/Co_{HCP} ratio in WC–Co cemented carbides has been challenging [9–12]. One bottleneck is that the soft Co phase is prone to excessive removal compared to the WC phase, leading to the inferior indexability of the Co phase using electron backscatter diffraction (EBSD) [13,14]. Electro-polishing is highly suitable for mapping the Co phase using EBSD. However, the WC hard phase and Co soft phase exhibit contrasting electrochemical behaviours: Co tends to remain stable and passive in alkaline environments, while WC demonstrates greater nobility in acidic solutions [15]. Furthermore, the significant disparity in the galvanic interaction between the Co and WC phases in WC–Co cemented carbides leads to a considerable challenge for electro-polishing as a method of metallographic preparation for EBSD analysis [16–18].

The other bottleneck is the ambiguity arising from the possibility of

* Corresponding author at: School of Aerospace, Mechanical and Mechatronic Engineering, The University of Sydney, Sydney, NSW 2006, Australia.
E-mail address: simon.ringer@sydney.edu.au (S.P. Ringer).

https://doi.org/10.1016/j.matchar.2025.114915
Received 4 October 2024; Received in revised form 22 February 2025; Accepted 7 March 2025
Available online 9 March 2025

introducing a Co phase transformation during metallographic preparation. Co_{FCC} can undergo a displacive deformation-induced phase transformation to its Co_{HCP} allotrope during metallographic processes at ambient temperatures [19–23]. This situation can introduce ambiguity as to whether the observed Co_{HCP} phase is pristine (i.e., the original phase) or an artefact arising from the metallographic preparation [24,25].

Mechanical polishing has been found to easily trigger the martensitic Co_{FCC}–Co_{HCP} phase transformation. Yang et al. revealed that mechanical polishing methods trigger the martensitic Co_{FCC}–Co_{HCP} phase transformation between 0 and 5 μm below the surface in the WC–13Co cemented carbide with a mean WC grain size of 0.7 μm [24]. Mingard et al. [25] also found that mechanical polishing methods led to the martensitic Co_{FCC}–Co_{HCP} phase transformation in more fine-grained WC–Co microstructures as opposed to the coarser WC grain sizes (larger than ~3 μm).

To tackle such issues, ion polishing has emerged as an important metallographic preparation method for advanced materials characterisation [5,13,26–29]. Broad argon ion (Ar^+) polishing has been reported to maintain the pristine Co phase in the coarse-grained WC–11Co cemented carbides with WC grain size larger than 5 μm [30]. The application of Xenon ion (Xe^+) plasma focused ion beam (pFIB) at 30 kV and 59 nA has been demonstrated to suppress the martensitic Co_{FCC}–Co_{HCP} phase transformation in the WC–11Co cemented carbides with 1–15 μm WC grain sizes [31]. However, there is still a knowledge gap regarding the suppression of the martensitic Co_{FCC}–Co_{HCP} phase transformation during metallographic preparation when the WC grain is smaller than 1 μm [32].

In this study, we propose a comprehensive metallographic method aimed at an accurate identification of the Co phase in both coarse and fine-grained WC–Co cemented carbides. We systematically compare and critique the efficacy of various metallographic preparation workflows, encompassing both for plane-polished cross-sections used for EBSD analysis, as well as for thin-sections such as used for TEM analysis. Our results illuminate the complex challenges inherent in accurately discerning the pristine Co phase, a determination vital for the subsequent analysis of microstructure and properties in WC–Co cemented carbides.

2. Experimental

We investigated two cemented carbides WC–10Co and WC–10Co–1.5Ru–0.6Cr_3C_2 (all compositions in the following are in wt %) from CERATIZIT Luxembourg S. à r.l., and a 99.99 % Co button. The nominal WC grain sizes of the WC–10Co and WC–10Co–1.5Ru–0.6Cr_3C_2 were 1.3–2.5 μm (coarse-grained) and 0.5–0.8 μm (fine-grained), respectively. Initial sample sectioning was conducted with a diamond saw, followed by a graded grind process using SiC abrasive papers at 30, 15, and 8 μm granulations. Subsequent polishing employed diamond particles at 6, 3, and 1 μm, and colloidal silica at 0.04 μm, using an Allied Hightech MultiPrep tool. The samples subjected to this preparation process are henceforth designated as "mechanical polishing". These "mechanically polished" samples were further polished by the PELCO® Tripod Polisher™ 59 using 15, 9, 3, 1, and 0.2 μm diamond films and these are designated as "mechanical polishing plus tripod polishing". A comprehensive description of the mechanical and tripod polishing protocols is presented in Table 1.

As a non-destructive technique, the X-ray diffraction (XRD) technique was conducted to accurately identify the crystalline structure of the Co phase in the "only mechanically polished", and "mechanically polished plus tripod polished" samples using a PANalytical X'Pert Powder flat plate system in the θ–2θ configuration with Cu-Kα radiation. The crystalline structures of the Co phase identified by XRD are considered the baseline, i.e., the pristine structure of the Co phase, for the WC–10Co and WC–10Co–1.5Ru–0.6Cr_3C_2 cemented carbides, and the Co button, respectively.

Table 1
Detailed procedures and polishing parameters for the mechanical polishing and tripod polishing.

Mechanical polishing at ambient temperature (27 °C)			Tripod polishing at ambient temperature (27 °C)	
Grinding				
Particle size (μm)		Loading stress (MPa)	Diamond polishing particle size (μm)	
Step 1	30		Step 1	15
Step 2	15	~ 0.1	Step 2	9
Step 3	8		Step 3	3
Diamond polishing				
Particle size (μm)		Loading stress (MPa)	Step 4	1
Step 4	6		Step 5	0.2
Step 5	3	~ 0.1	Step 6	0.04 OPS solution
Step 6	1			
Step 7	0.04 OPS solution			

To achieve a high-quality surface and to suppress the martensitic Co_{FCC}–Co_{HCP} phase transformation in the fine-grained WC–10Co–1.5Ru–0.6Cr_3C_2 cemented carbides, a comparative assessment of various metallographic preparation workflows was conducted. These workflows encompass solely mechanical polishing (c.f. Table 1) as well as combined technique of the mechanical polishing followed by broad Ar^+ ion polishing. The samples prepared using the combined approach are designated as "mechanically polished plus broad Ar^+ ion polished" for plane-polished cross-sections used in (e.g.) EBSD analysis. The precise configurations for the broad Ar^+ ion polishing, such as beam energy, beam current, and glancing angle, are detailed in Table 2. Detailed configurations of broad Ar^+ ion polishing as an additional sample preparation method used for plane-polished cross-sections used in (e.g.) EBSD analysis.

To suppress charging effects during analytical procedures, which can distort and degrade imaging quality, conductive silver paint was applied. Microstructural analyses of these samples were performed using EBSD techniques on a Zeiss Ultra Plus field-emission gun scanning electron microscope (SEM) operating at 20 kV and with an aperture size of 120 mm.

To prepare thin films for transmission electron microscopy (TEM) or transmission Kikuchi diffraction (TKD), the fine-grained WC–10Co–1.5Ru–0.6Cr_3C_2 cemented carbides were initially sectioned using a diamond saw. To effectively suppress the martensitic Co_{FCC}–Co_{HCP} phase transformation during the subsequent preparation stages, diverse workflows were implemented for thin-sections such as used in (e.g.) TEM analysis. Following sample sectioning, thin-sections were subjected to either tripod polishing coupled with precision Ar^+ ion polishing (designated as "mechanically polished plus tripod polished

Table 2
Detailed configurations of broad Ar^+ ion polishing as an additional sample preparation method used for plane-polished cross-sections used in (e.g.) EBSD analysis.

Broad Ar^+ ion polishing configuration 1 (~10 MJ/m^2 and 80 min) at ambient temperature (27 °C)				
	Beam energy (keV)	Ion current (μA)	Time (min)	Polish angle (°)
Step 1	8	80	60	± 5
Step 2	2	15	10	± 5
Step 3	0.5	10	10	± 5
Broad Ar^+ ion polishing configuration 2 (~21.65 MJ/m^2 and 420 min) at ambient temperature (27 °C)				
	Beam energy (keV)	Ion current (μA)	Time (min)	Polish angle (°)
Step 1	6	65	60	± 5
Step 2	4.5	35	60	± 5
Step 3	3.5	20	60	± 5
Step 4	2.5	10	60	± 5
Step 5	1.5	10	60	± 5
Step 6	1	10	60	± 5
Step 7	0.5	10	60	± 5

plus precision Ar^+ ion polished"), Xe^+ pFIB using ambient temperature thinning configuration (designated as "ambient Xe^+ pFIB prepared"), or Xe^+ pFIB configuring the thinning temperature at approximately −195 °C (designated as "Cryogenic Xe^+ pFIB prepared"). Further details of these workflows are provided in.

This study aims to identify metallographic preparation workflows that effectively ensure the surface quality and suppress the martensitic Co_{FCC}–Co_{HCP} phase transformation in the fine-grained WC–10Co–1.5Ru–0.6Cr_3C_2 cemented carbides for the plane-polished cross-sections used in (e.g.) EBSD analysis.

Table 3. These preparation variations aimed to optimise results and minimise the occurrence of the martensitic Co_{FCC}–Co_{HCP} phase transformation in the final TEM analysis.

The thin-sections' microstructures, prepared using different workflows, were characterised using TKD. TKD mapping was performed on the same platform and configurations as EBSD-SEM, with step sizes of 10 nm and 5 nm respectively, and an Oxford Nordlys Nano EBSD detector. Results were processed using the Oxford Instruments AZtec 2.0 EBSD software and the data was post-processed using HKL Channel-5 software package. The Co phase identification within the thin-sections was further verified using a two-dimensional fast Fourier transform (2D-FFT) method under high resolution TEM (HRTEM). Both 2D-FFT and bright-field TEM images were acquired with a ThermoFisher Spectra TEM operated at an acceleration voltage of 300 kV.

This study aims to identify metallographic preparation workflows that effectively ensure the surface quality and suppresses the martensitic Co_{FCC}–Co_{HCP} phase transformation in the fine-grained WC–10Co–1.5Ru–0.6Cr_3C_2 cemented carbides for the plane-polished cross-sections used in (e.g.) EBSD analysis.

3. Results

3.1. Precise identification of the pristine Co structure using XRD technology

Our XRD outcomes, depicted in Fig. 1(a), shows that only Co_{HCP} phase is present in the "mechanical polishing only" WC–10Co–1.5Ru–0.6Cr_3C_2 sample, whilst both the Co_{FCC} phase and Co_{HCP} phase in the "mechanically polished plus tripod polished" WC–10Co–1.5Ru–0.6Cr_3C_2 sample are present. This discrepancy might be attributed to two possibilities. The first one is that tripod polishing inducing Co_{HCP}–Co_{FCC} phase transformation, indicating a HCP pristine structure for the Co phase. The other possibility is that tripod polishing effectively removes the Co_{HCP} phase in the deformed region near the surface induced by "mechanical polishing only", suggesting an FCC pristine structure for the Co phase.

To scrutinise the aforementioned explanations, a comparative analysis was conducted between the 99.99 % Co button and the WC–10Co cemented carbide. As illustrated in Fig. 1**(b-c)**, no Co_{FCC} phase was detected in both the "only mechanically polished" and the "mechanically polished plus tripod polished" Co and WC–10Co samples. This observation strongly suggests that the occurrence of the martensitic Co_{FCC}–Co_{HCP} phase transformation during tripod polishing is highly improbable. Moreover, considering that Co_{HCP} is stable at ambient temperature and unlikely to transform to the Co_{FCC} phase [32], it is inferred that the tripod polishing effectively removes the Co_{HCP} phase from the deformed regions near the top surface induced by the sectioning and mechanical polishing. Hence, it can be concluded that the pristine structure of the Co phase in the WC–10Co–1.5Ru–0.6Cr_3C_2 cemented carbides is FCC. Simultaneously, it was deduced that mechanical polishing initiates the martensitic Co_{FCC}–Co_{HCP} phase transformation in the WC–10Co–1.5Ru–0.6Cr_3C_2 cemented carbides.

3.2. Validation of the metallographic preparation workflow on the pristine Co structure for plane-polished cross-sections used in (e.g.) EBSD analysis

To prepare for plane-polished cross-sections used in (e.g.) EBSD analysis, grinding and mechanical polishing was used to maintain a mirror-like surface firstly. Detailed procedures and parameters are outlined in Table. 1. Acknowledging that mechanical polishing may induce the martensitic Co_{FCC}–Co_{HCP} phase transformation, it became evident that the Co structure in the fine-grained WC–10Co–1.5Ru–0.6Cr_3C_2 cemented carbide, prepared through this method, does not faithfully represent the pristine Co structure for microstructural analysis. To mitigate this issue, additional preparation methods, such as broad Ar^+ ion polishing, are deemed necessary to eliminate the artefactual Co_{HCP} phase generated during the mechanical polishing. Subsequently, a comprehensive series of EBSD analyses were conducted on the "mechanically polished plus broad Ar^+ ion polished" surface and compared to the results obtained from the "only mechanically polished" surface, as depicted in Fig. 2.

The band contrast map, overlapped with the Co phase mapping for the "only mechanically polished" surface depicted in Fig. 2(a_1) and the "mechanically polished plus broad Ar^+ ion polished" surface shown in Fig. 2(b_1), demonstrate a notable discrepancy in the statistical phase fractions of the Co structures. Specifically, 43.05 % and 56.95 % of the Co phase were identified as Co_{FCC} and Co_{HCP}, respectively, in the WC–10Co–1.5Ru–0.6Cr_3C_2 sample prepared by mechanical polishing only. In contrast, for the sample prepared with broad Ar^+ ion polishing, a substantial majority of the Co phase (96.11 %) was identified as Co_{FCC} phase. Given the XRD results affirming the pristine Co phase in the WC–10Co–1.5Ru–0.6Cr_3C_2 cemented carbide, it is inferred that broad Ar^+ ion polishing effectively eliminates the artefactual Co_{HCP} phase introduced by mechanical polishing. Therefore, a combined approach of "mechanical polishing and broad Ar^+ ion polishing" emerges as an optimal metallographic workflow to accurately preserve the pristine Co structure in WC–10Co–1.5Ru–0.6Cr_3C_2 cemented carbide.

To elucidate the insights of this martensitic Co_{FCC}–Co_{HCP} phase transformation process, inverse pole figure–Z (IPF–Z) colouring maps, as displayed in Fig. 2(a_3-a_4) and Fig. 2(b_3-b_4), were characterised. These maps reveal that the area identified as the parent Co_{FCC} phase possesses a single crystallographic orientation. Conversely, the newly formed

Table 3
Detailed specifies of the preparation workflows used for thin-sections such as used in (e.g.) TEM analysis.

Workflow 1					Workflow 2	Workflow 3
Step 1	Tripod polishing (c.f. Table 1) at ambient temperature (27 °C)				Step 1	Mechanical polishing (c.f. Table 1) at ambient temperature (27 °C)
Step 2	Precision Ar^+ ion polishing at ambient temperature (27 °C)				Step 2	Broad Ar^+ ion polishing (c.f. Table 2. **Detailed configurations of broad Ar^+ ion polishing as an additional sample preparation method used for plane-polished cross-sections used in (e.g.) EBSD analysis.**) at ambient temperature (27 °C)
	Beam energy (KeV)	Ion current (μA)	Time (min)	Polish angle (°)	Step 3	Ambient Xe^+ pFIB (27 °C)	Cryogenic Xe^+ pFIB (−196 °C)
	8	110	75	± 8		Xe^+ lift out + thinning under ambient temperature	Xe^+ lift out + thinning under cryogenic temperature
	3	30	15	± 4			
	0.3	25	15	± 4			

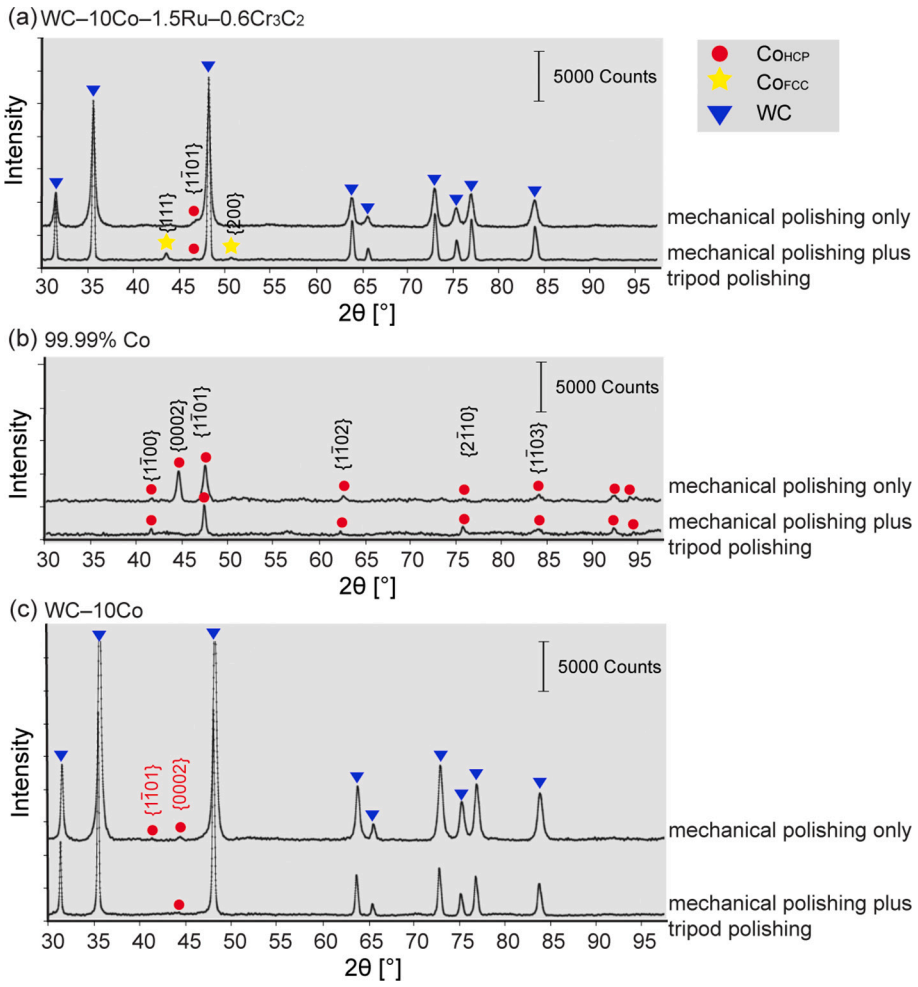

Fig. 1. Identification of the pristine Co phase in (a) WC–10Co–1.5Ru–0.6Cr_3C_2, (b) 99.99 % Co, and (c) WC–10Co samples, respectively, using XRD. "Only mechanically polished", and "mechanically polished plus tripod polished" surfaces are compared.

Co_{HCP} phase presents crystallographic misorientations with highly refined grain sizes, aligning with findings reported in the existing literature [24]. Further insights are provided by the pole figures in Fig. 2 (a_5) and (b_5), which detail the crystallographic directions of the Co phases, thereby illustrating the martensitic Co_{FCC}–Co_{HCP} phase transformation mechanism. These findings demonstrate that both the artefactual Co_{HCP} structure and the pristine Co_{FCC} structure follow the Shoji-Nishiyama orientation relationship, i.e., {111} ⟨110⟩ Co_{FCC} // {0001} $<11\bar{2}0>$ Co_{HCP}, indicating that the detected Co_{HCP} regions with multiple variants arise from a single crystallographic Co_{FCC} parent grain [33].

3.3. *Validation of the metallographic preparation workflow on the pristine Co structure for thin-sections such as used in (e.g.) TEM analysis*

Electro-polishing, ion polishing, and tripod polishing are widely recognised as prevalent techniques for the preparation of TEM lamellae [34]. However, the distinct electrochemical corrosion behaviours of the hard WC phase and the soft Co binders, being diametrically opposite [16,17], render electro-polishing unsuitable for the TEM sample preparation of the WC–Co cemented carbides. Consequently, such samples necessitate preparation via alternative methods, including tripod polish followed by the precision ion polishing method, or conventional mechanical polishing followed by the advancements of multiple ion polishing techniques, such as FIB. It is worthwhile mentioning that FIB can introduce artefacts that potentially modify or damage the sample structures, contingent upon the ion energy and the incident angles [31,35,36]. Therefore, a critical assessment is essential to appropriateness of these techniques' workflows for the fine-grained WC–Co cemented carbides, specifically regarding the preservation of the pristine Co structure.

In this work, the first metallographic workflow proposed for TEM analysis encompasses "mechanical polishing plus tripod polishing plus precision Ar^+ ion polishing", with details presented in.

This study aims to identify metallographic preparation workflows that effectively ensure the surface quality and suppresses the martensitic Co_{FCC}–Co_{HCP} phase transformation in the fine-grained WC–10Co–1.5Ru–0.6Cr_3C_2 cemented carbides for the plane-polished cross-sections used in (e.g.) EBSD analysis.

Table 3 under "Method 1". Based on our XRD findings, the application of the tripod mechanical polishing has been confirmed to facilitate the preservation of the pristine Co structure in the WC–10Co–1.5Ru–0.6Cr_3C_2 cemented carbide. The subsequent impact of precision Ar^+ ion polishing on the metallographic artefacts in the WC–10Co–1.5Ru–0.6Cr_3C_2 samples was further explored. As shown in Error! Reference source not found., TKD results derived from surfaces processed via "mechanical polishing plus tripod polishing plus precision Ar^+ ion polishing" showcase high-quality imaging with high indexing rates. Phase mapping presented in Fig. 3(a_1) reveals an 88.30 % presence of the Co_{FCC} phase, with a minimal fraction of the Co_{HCP} phase. This thereby suggests that precision Ar^+ ion polishing method effectively preserved the pristine Co_{FCC} structure. These results align with those obtained from XRD, evidencing a concordance between the two

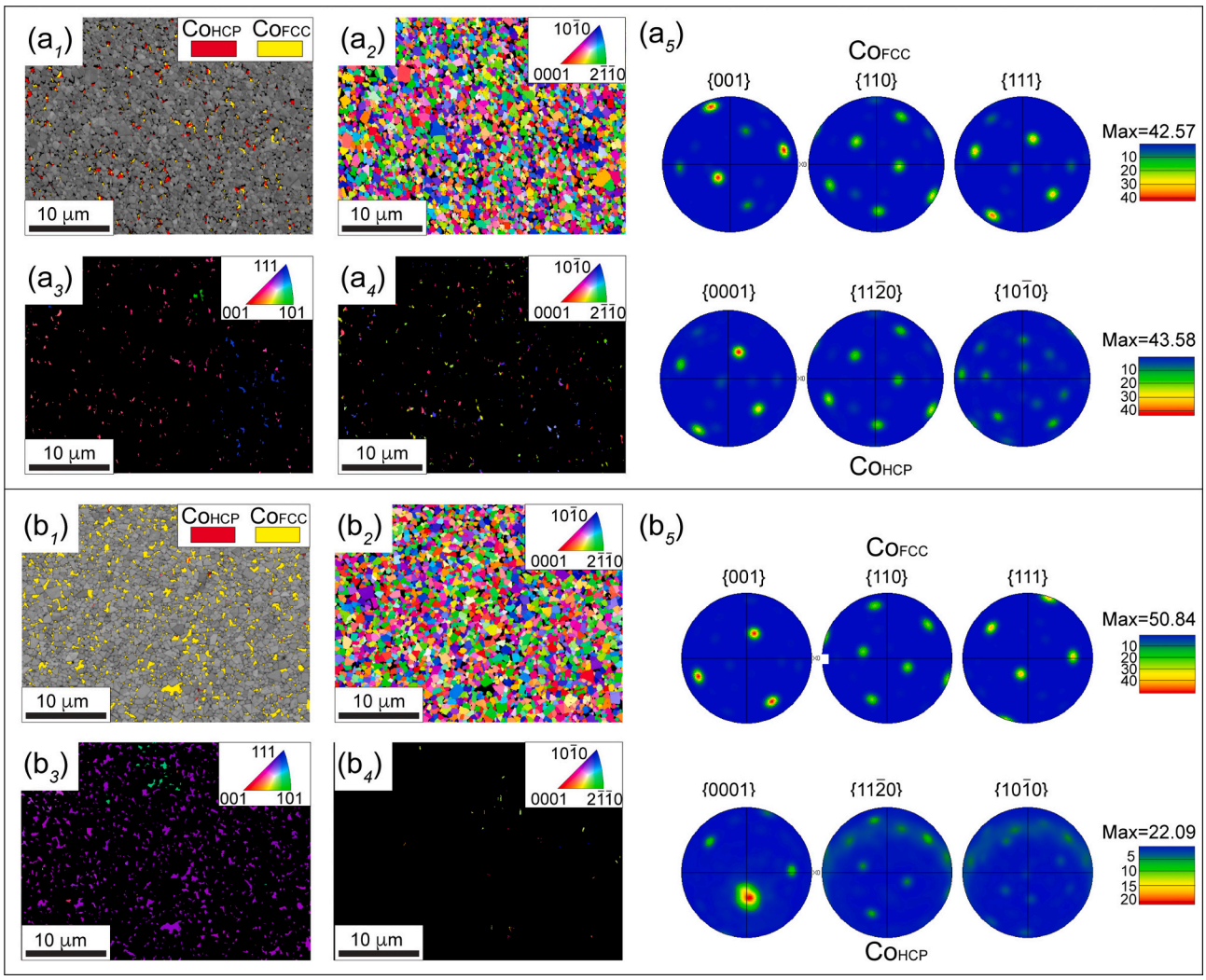

Fig. 2. Examination of the broad Ar^+ ion polishing on the suppression of the martensitic Co_{FCC}–Co_{HCP} phase transformation. EBSD analysis on the (a) "only mechanically polished", and (b) "mechanically polished plus broad Ar^+ ion polished" WC–10Co–1.5Ru–0.6Cr_3C_2 samples. (a_1) and (b_1) are the phase maps overlapped with the band contrast. Co_{HCP} and Co_{FCC} are indexed in red and yellow, respectively. IPF–Z maps of (a_2) and (b_2) WC grains, (a_3) and (b_3) Co_{FCC}, and (a_4) and (b_4) Co_{HCP}. (a_5) and (b_5) are the pole figures of the Co_{FCC} and Co_{HCP} phases. (For interpretation of the references to colour in this figure legend, the reader is referred to the web version of this article.)

analytical methods. HRTEM observations presented in Fig. 3(b), including the interfacial structures of WC/Co, alongside 2D-Fast Fourier Transform (2D-FFT) patterns, elucidate the orientation relationship between WC_{HCP} and Co_{FCC}, i.e., $(01\bar{1}0)[\bar{2}110]$ WC_{HCP} //$(11\bar{1})[011]$ Co_{FCC}. These observations further confirm the crystallographic structure information of the Co phase within the sample, i.e., Co_{FCC} structure.

The examination of the artefactual Co phase alterations within the fine-grained WC–Co cemented carbides was conducted using advanced plasma FIB-based TEM preparation techniques, specifically "ambient Xe^+ pFIB" and "cryogenic Xe^+ pFIB", respectively. The detailed procedures are documented in.

This study aims to identify metallographic preparation workflows that effectively ensure the surface quality and suppresses the martensitic Co_{FCC}–Co_{HCP} phase transformation in the fine-grained WC–10Co–1.5Ru–0.6Cr_3C_2 cemented carbides for the plane-polished cross-sections used in (e.g.) EBSD analysis.

Table 3 as "Workflow 2" and "Workflow 3". To preserve the pristine Co_{FCC} structure, samples earmarked for pFIB analysis were initially subjected to the "mechanical polishing plus broad Ar^+ ion polishing" methods. This preparation approach was previously confirmed as effective in preserving the pristine Co phase, as discussed in the preceding sections.

The TKD analyses of the samples prepared using ambient Xe^+ pFIB and cryogenic Xe^+ pFIB are showcased in Fig. 4(a) and (b), respectively. The corresponding phase maps, Fig. 4(a_1) and Fig. 4(b_1), highlight the Co_{FCC} structure in red and Co_{HCP} structure in yellow. Notably, 29.91 % of the Co phase was identified as Co_{FCC} in Fig. 4(a_1), whereas Fig. 4(b_1) displayed almost no Co_{FCC}. This statistical phase fraction analysis demonstrates that both "ambient Xe^+ pFIB" and "cryogenic Xe^+ pFIB" facilitated the martensitic Co_{FCC}–Co_{HCP} phase transformation.

Contrary to the beneficial effects observed with cryogenic FIB in other contexts, particularly in the field of biological sciences [36,37], the application of "cryogenic Xe^+ pFIB" in this study led to an unfavourable outcome by promoting the martensitic Co_{FCC}–Co_{HCP} phase transformation. The IPF–Z colouring maps, depicted in Fig. 4(a_2-a_4) and Fig. 4(b_2-b_4), show that the parent Co_{FCC} phase maintains a single crystallographic orientation, whereas the newly formed Co_{HCP} phase exhibits multiple crystallographic orientations. This variability suggests that the Co_{FCC} grains transform into several different Co_{HCP} variants as there are 12 shear orientations of the Co_{FCC} structure available to this transformation.

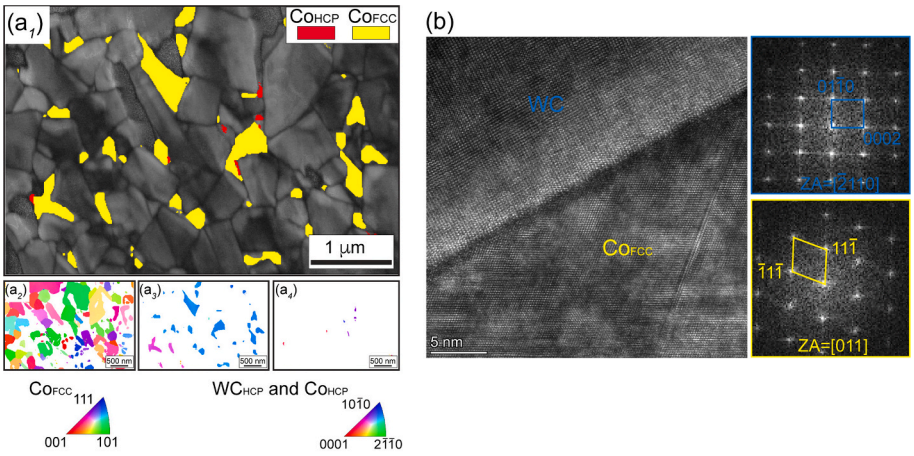

Fig. 3. Examination of the precision Ar^+ ion polishing on the suppression of the martensitic Co_{FCC}–Co_{HCP} phase transformation. (a) TKD and (b) HRTEM analyses of the "mechanically polished plus tripod polished plus precision Ar^+ ion polished" WC–10Co–1.5Ru–0.6Cr_3C_2 TEM samples. (a_1) phase map overlapped with band contrast where Co_{HCP} and Co_{FCC} are indexed in red and yellow, respectively. IPF–Z maps of the WC grains, Co_{FCC}, and Co_{HCP} are shown in ($a_{2–4}$), respectively. (b) HRTEM image of both WC_{HCP} and Co_{FCC} regions with corresponding 2D-FFT patterns. (For interpretation of the references to colour in this figure legend, the reader is referred to the web version of this article.)

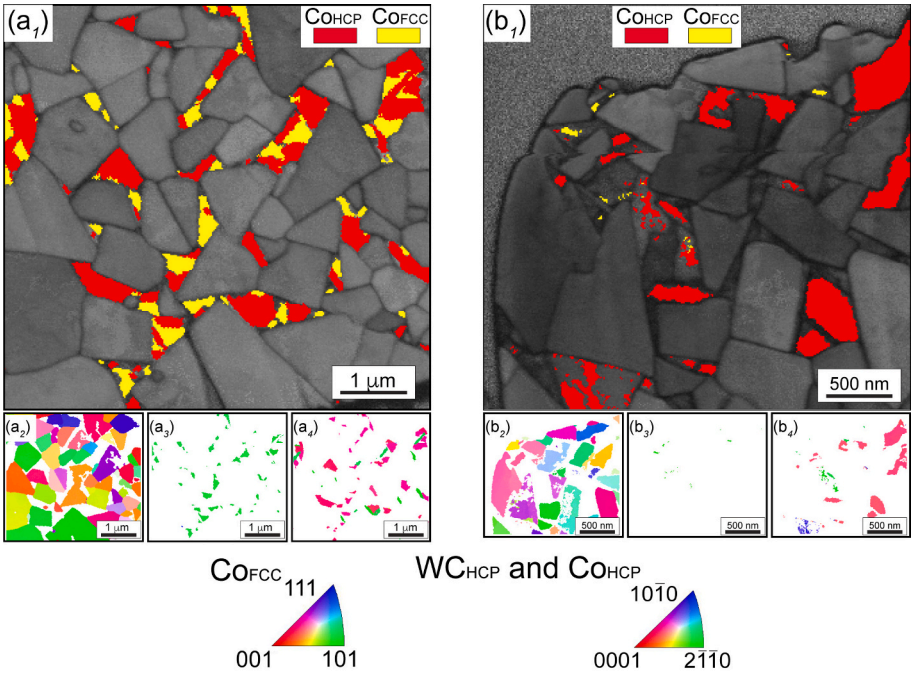

Fig. 4. Temperature effect during Xe^+ pFIB polishing on the suppression of the martensitic Co_{FCC}–Co_{HCP} phase transformation. (a) Ambient and (b) cryogenic condition. The preparation protocol for both cases is the same, which is "mechanically polished plus broad Ar^+ ion polished sample from Fig. 3(b).

3.4. Effect of mechanical polishing cloths on EBSD indexability

Mechanical polishing with diamond abrasives is regarded a pivotal step in metallographic preparation, essential for removing scratches and plastic deformation incurred during prior grinding stages. The choice of the mechanical polishing cloths significantly influences the abrasive particles" movement in the vertical direction, thereby affecting the effectiveness of the polishing process. To assess the effect of the mechanical polishing cloth types on the indexability of the backscattered diffraction signal and surface quality of the fine-grained WC–Co samples, a comparative analysis was conducted between the surfaces polished using a soft polishing cloth, i.e., MD-Mol, and a hard polishing cloth, i.e., MD-Dac, respectively.

Observations from Fig. 5**(a_1-a_2)** indicate a substantial presence of non-indexable Co phase and lower surface quality if polished using MD-Mol. Conversely, the surface polished with MD-Dac, as shown in Fig. 5 **(b_1-b_3)**, achieves superior backscattered diffraction signal indexing of both the WC and Co phases. Specifically, unindexed points are reduced from approximately 23.24 % (using soft MD-Mol cloth) to about 13.33 % (using hard MD-Dac cloth) in terms of area fractions. Notably, the indexed Co signals obtained with the hard cloth were approximately 4.8 times higher than those achieved using the soft cloth. This methodological refinement enables more accurate and representative measurements of the phase fractions in the WC–Co cemented carbide samples. Low EBSD indexability often results from excessively deformed surfaces or a high density of surface defects [38]. Using a soft polishing cloth leads to an increased movement in the vertical direction and therefore more pronounced surface deformation. This process tends to completely

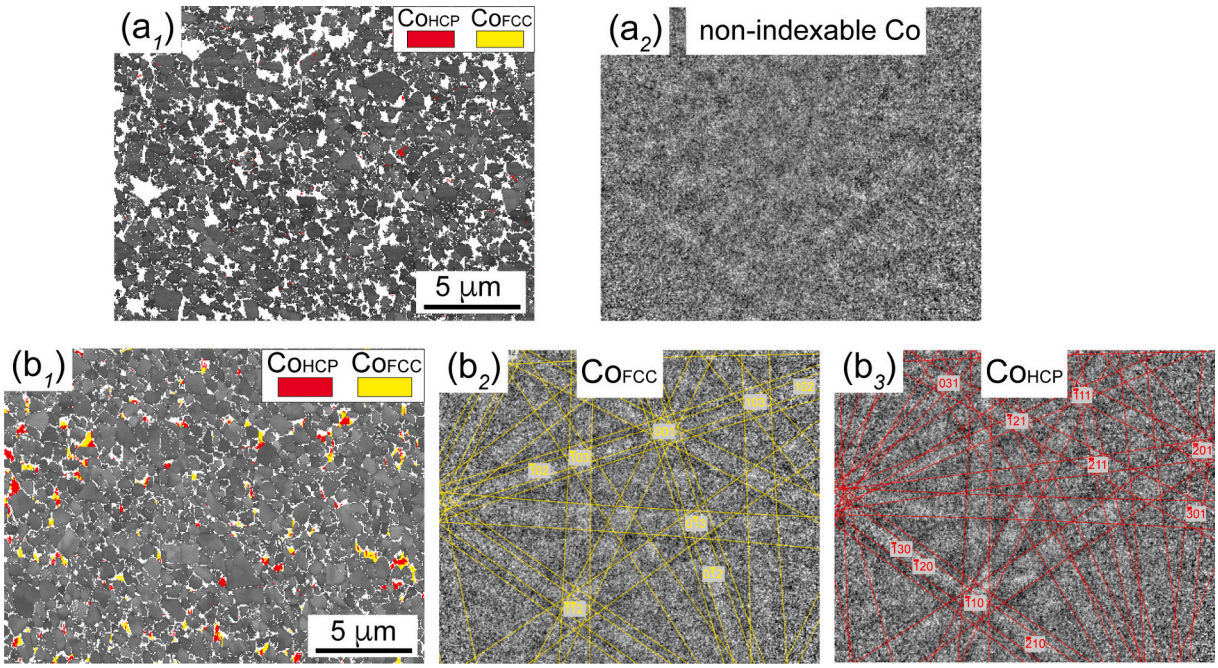

Fig. 5. Effect of mechanical polishing cloth types on the EBSD indexability and suppression of the martensitic Co_{FCC}–Co_{HCP} phase transformation. EBSD analysis of the "only mechanically polished" WC–10Co–1.5Ru–0.6Cr_3C_2 samples using a (a) soft polishing cloth and a (b) hard polishing cloth. (a_1) and (b_1) are the phase maps overlapped with the band contrast. Co_{HCP} and Co_{FCC} are indexed in red and yellow, respectively. (a_2), (b_2) and (b_3) are the detected electron backscattered Kikuchi patterns of Co regions with simulated indexing. (For interpretation of the references to colour in this figure legend, the reader is referred to the web version of this article.)

remove the softer Co phase from the surface layer while deforming the harder WC phase.

Remarkably, both Co_{FCC} and Co_{HCP} phases were identified in the electron backscattered patterns (EBSPs) of the fine-grained WC–10Co–1.5Ru–0.6Cr_3C_2 samples in Fig. 5**(b_2-b_3)**. This indicates the occurrence of preparation artefacts in the Co phase due to mechanical polishing. Thus, despite optimising EBSD indexability with a hard polishing cloth, artefactual Co_{HCP} was still observed. This highlights the necessity of integrating broad Ar^+ ion polishing to eliminate the deformed areas and preserve the pristine Co structures effectively.

3.5. *Effect of broad Ar^+ ion polishing configurations on modifications of the pristine Co_{FCC} structure*

As mentioned above, mechanical polishing tends to trigger the deformation-induced martensitic Co_{FCC}–Co_{HCP} phase transformation. Additional broad Ar^+ ion polishing was used to mitigate this effect. However, various configurations of the broad Ar^+ ion polishing may also trigger the deformation-induced martensitic phase transformation rather than mitigate these artefacts. It is therefore highly significant to quantitatively evaluate the effect of various ion polishing parameters that can be controlled such as beam current, beam power and duration on the preservation of the pristine Co_{FCC} structure.

Here, two distinct configurations with controllable beam parameters were assessed:"Ar^+ ion polishing configuration 1 (~10 MJ/m^2 and 80 min)", using 8 keV for 1 h followed by 2 keV and 0.5 keV for 10 min each; and a "Ar^+ ion polishing configuration 2 (~21.65 MJ/m^2 and 420 minutes)", which involves a gradually reducing beam power from 6 keV to 0.5 keV over a total duration of 7 h).

The statistical evaluation of the indexing rates and the phase fraction from the surfaces prepared with the aforementioned ion polishing configurations, i.e., "Ar^+ ion polishing configuration 1 (~10 MJ/m^2 and 80 minutes)", is detailed in Fig. 6. The analysis reveals that both configurations reduce non-indexed signals than those achieved through mechanical polishing alone. This thus suggests that broad Ar^+ ion polishing is effectively further improving the EBSD indexability of the sample prepared by the mechanical polishing. Furthermore, "Ar^+ ion polishing configuration 1 (~10 MJ/m^2 and 80 min)" was found to mitigate artefacts and eliminate the martensitic Co_{FCC}–Co_{HCP} phase transformation. Quantitatively, 96.11 % of the Co phase was identified as Co_{FCC} in the WC–10Co–1.5Ru–0.6Cr_3C_2 sample subjected to the "Ar^+ ion polishing configuration 1 (~10 MJ/m^2 and 80 min)". Conversely, the surface prepared using the "Ar^+ ion polishing configuration 2 (~21.65 MJ/m^2 and 420 minutes)" exhibits a significant presence of the Co_{HCP} artefacts, as illustrated in Fig. 6(b).

The comparative analysis of the phase fraction for the two broad Ar^+ ion polishing configurations highlights that using a higher beam power and higher current coupled with a shorter polishing duration is more effective in eradicating deformed WC and Co layers without triggering the martensitic Co_{FCC}–Co_{HCP} phase transformation. On the other hand, a gentler beam power and beam current with prolonged polishing duration resulted in additional artefacts and surface damage. While the "Ar^+ ion polishing configuration 2 (~21.65 MJ/m^2 and 420 minutes)" can be advantageous for many other materials in terms of surface quality for microscopy, it proves unsuitable for our fine-grained WC–Co cemented carbides, especially in the presence of a metastable Co_{FCC} structure.

3.6. *Effect of Xe^+ plasma milling temperature on modifications of the pristine Co_{FCC} structure*

FIB offers significant advantages, including the precise, site-specific removal of material from small regions with high spatial resolution [39]. In this study, sample preparation with Xe^+ pFIB, thinning at ambient or cryogenic temperatures, has been observed to induce the martensitic Co_{FCC}–Co_{HCP} phase transformation. Notably, a portion of the Co regions managed to preserve the Co_{FCC} structure following preparation with ambient Xe^+ pFIB. The question about the integrity of these Co_{FCC} regions as "unmodified" pristine structure and their suitability for microstructural characterisations raises.

Pole figures of both Co_{FCC} and Co_{HCP} phases from Xe^+ pFIB-prepared

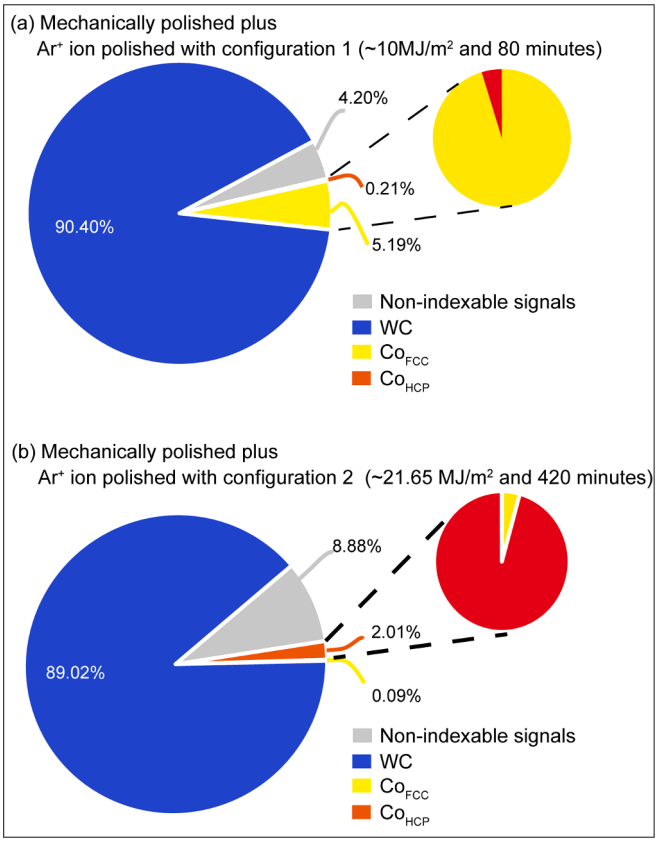

Fig. 6. Effect of the broad Ar^+ ion polishing configurations on the modifications of the pristine Co_{FCC} structure. EBSD measurements on the fractions of the non-indexable signals, WC, Co_{HCP} and Co_{FCC} structures of the (a) "mechanically polished plus Ar^+ ion polished with configuration 1 (~10 MJ/m^2 and 80 minutes) " and (b) "mechanically polished plus Ar^+ ion polished with configuration 2 (~21.65 MJ/m^2 and 420 minutes) " WC–10Co–1.5Ru–0.6Cr_3C_2 samples.

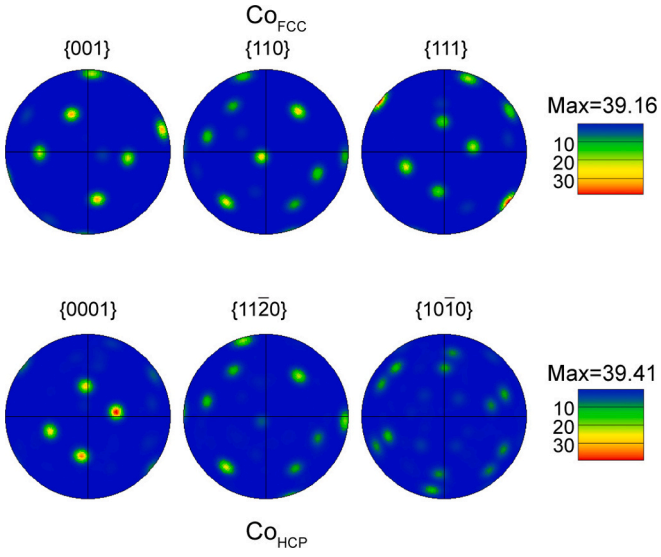

Fig. 7. Examination on the "ambient Xe^+ pFIB prepared" on suppression of the martensitic Co_{FCC}–Co_{HCP} phase transformation. Pole figures of the both Co_{FCC} and Co_{HCP} phases in the "mechanically polished plus broad Ar^+ ion polished configuration 1 (~10 MJ/m^2 and 80 minutes) plus ambient Xe^+ pFIB prepared" WC–10Co–1.5Ru–0.6Cr_3C_2 cemented carbides. The corresponding phase maps overlapped with the band contrast and IPF – Z maps are presented in Fig. 4 **(a_1-a_4)**.

samples, as shown in Fig. 7, reveal that the Co_{FCC} grains transform into several distinct Co_{HCP} variants, adhering to the Shoji-Nishiyama orientation relationship, i.e., $\{111\}_{FCC}//\{0001\}_{HCP}$, and $\langle 110\rangle_{FCC}//<11\bar{2}0>_{HCP}$. Specifically, Fig. 7 illustrates that four crystallographically equivalent variants, characterised by four $\{0001\}_{HCP}$ basal planes stem from four $\{111\}_{FCC}$ habit planes [40], aligning with the findings in Fig. 2(b_5) from the samples prepared with "mechanical polishing plus broad Ar^+ ion polishing". This alignment verifies that the remaining Co_{FCC} represents the parent phase without modification.

Therefore, ambient Xe^+ pFIB emerges as a viable technique for microstructural characterisation, yet it necessitates cautious interpretation when quantifying the extent of pristine Co_{FCC} regions, to account for potential modifications induced by the preparation process.

3.7. Summary of the validated metallographic preparation workflow for the pristine Co phase identification

To provide a comprehensive understanding of the examinations conducted in this study, we present an overview of the metallographic preparation workflows, as detailed in Fig. 8. This figure highlights how various preparation methods contribute to achieving the desired surface quality for EBSD/TKD indexing and the suppression of the martensitic Co_{FCC}–Co_{HCP} phase transformation in fine-grained WC–10Co–1.5Ru–0.6Cr_3C_2 cemented carbides. Specifically, these metallographic preparation techniques are classified into three categories based on their effectiveness and appropriateness for our specific material: "Go", "No Go", and "Go with caution". "Go" signifies workflows that are safe and advocated for use, "No Go" represents workflows that should be avoided, and "Go with caution" indicates workflows that could be considered, provided that particular precautions are observed, following the detailed discussions and recommendations outlined in the study. This categorisation facilitates a clear understanding of the suitable preparation workflows for the fine-grained WC–10Co–1.5Ru–0.6Cr_3C_2 cemented carbides, ensuring reliable and accurate microstructural characterisation.

3.8. Effect of Ar^+ ion beam energy density and polishing duration on the suppression of the pristine Co_{FCC} structure

As mentioned above, controlling the beam parameters can effectively suppress the pristine Co_{FCC} structure and maintain good surface quality for EBSD analysis. To systematic study the effect of Ar^+ ion beam energy density and polishing duration on the suppression of the pristine Co_{FCC} structure, Fig. 9 displays a plot correlating ion polishing energy density with duration across four distinct broad Ar^+ ion polishing workflows. Each workflow involves multiple steps of applying ion beam energy density and polishing duration. The effectiveness of each polishing step was evaluated, categorising them as "Go" for satisfactory suppression of the martensitic transformation and superior surface quality, or "No Go" for inadequate outcomes, manifesting either through poor surface quality or the introduction of preparation artefacts. Energy density of the ion polishing can be determined from the beam power and beam current and the "Ar^+ ion polishing configuration 1" has an Ar^+ ion polishing energy density of ~10 MJ/m^2 and a duration of ~80 min. It is noted that polishing with such "Ar^+ ion polishing configuration 1 (~10 MJ/m^2 and 80 minutes)" or near these energy density and duration values are marked as "GO" step for EBSD analysis. Consequently, the "Ar^+ ion polishing configuration 1 (~10 MJ/m^2 and 80 min)" has been selected for our WC–Co cemented carbides to optimally preserve the pristine Co structure, as corroborated by the findings depicted in Fig. 3.

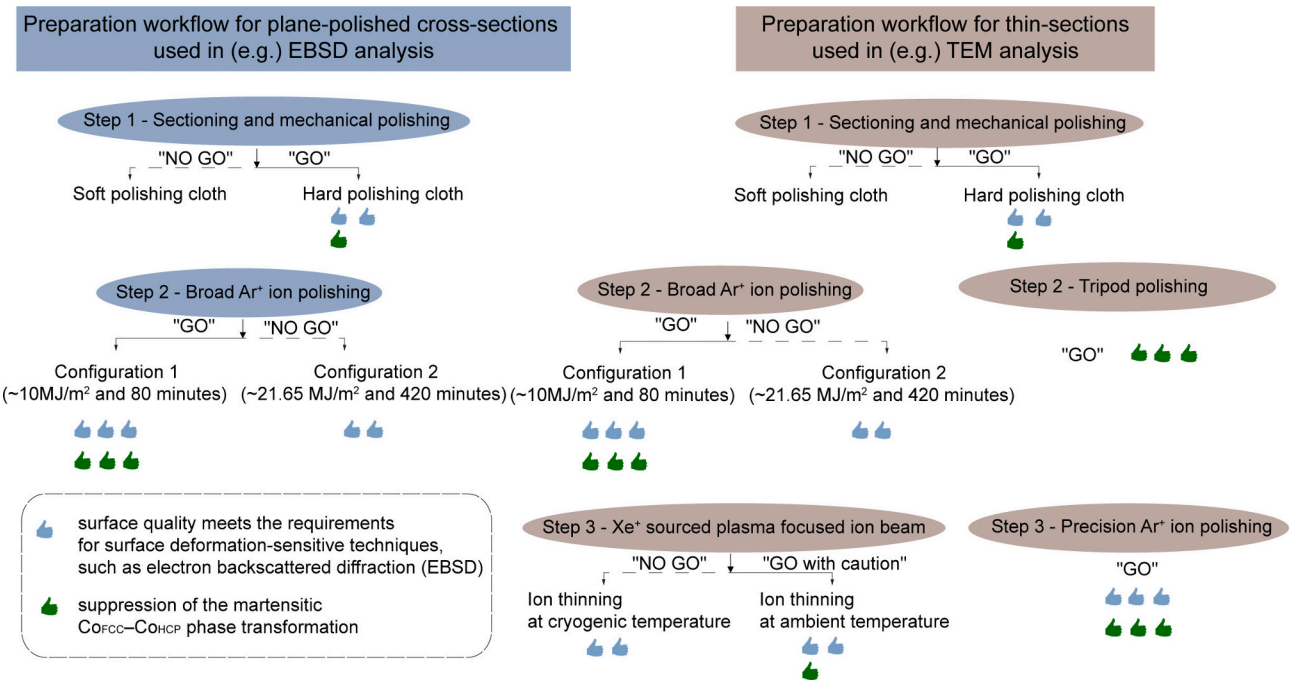

Fig. 8. Overview of the metallographic preparation workflows validated in this work with the following comments of each method: "Go", "NO GO" and "GO with caution".

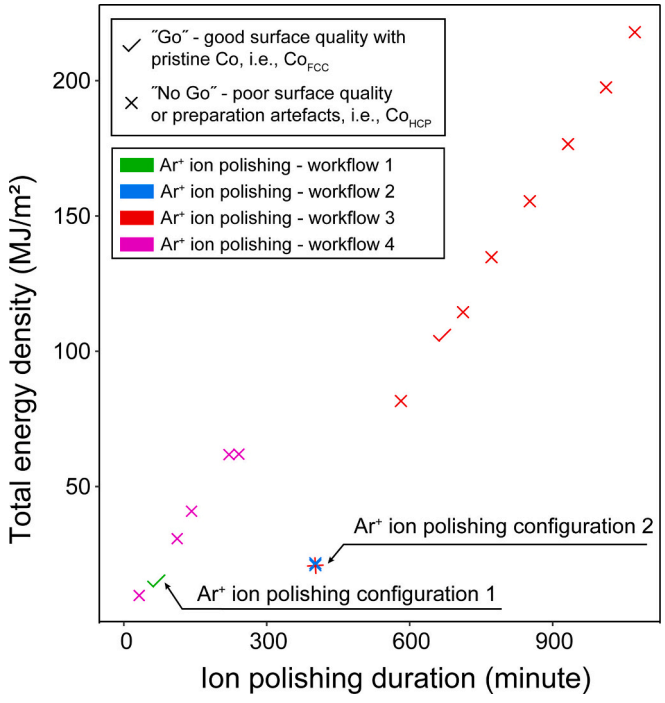

Fig. 9. Effect of the Ar^+ ion polishing energy density versus ion polishing duration on the preservation of the pristine Co phase in the WC–10Co–1.5Ru–0.6Cr_2C_3 cemented carbides. The total ion polishing energy density versus its duration after each step from four different broad Ar^+ ion polish workflows marked as "Ar^+ ion polishing - workflow 1" to "Ar^+ ion polishing - workflow 4"in green, blue, red and purple colours, respectively. "√ " and "×" represent "Go" and "No Go" ion polishing configurations, respectively. "GO" is regarded as safe configuration step, effectively suppressing the martensitic Co_{FCC} to Co_{HCP} phase transformation. "NO GO" is regarded as unsafe configuration step, providing insights into unexpected experimental consequences. (For interpretation of the references to colour in this figure legend, the reader is referred to the web version of this article.)

4. Discussion

4.1. Mechanism for minimizing the martensitic Co_{FCC}–Co_{HCP} phase transformation

Exploring the balance between ion polishing energy density and duration is crucial for optimising the preparation of WC–Co cemented carbides, especially in the context of suppressing the martensitic Co_{FCC}–Co_{HCP} phase transformation and achieving high EBSD indexing rates. In our study, various configurations of the broad Ar^+ ion polishing, including both "Ar^+ ion polishing configuration 1 (~10 MJ/m^2 and 80 minutes)" and "Ar^+ ion polishing configuration 2 (~21.65 MJ/m^2 and 420 minutes)", as well as combined approaches, were assessed to understand their influence on the phase transformation and the EBSD indexability.

The "No Go" outcomes were notably prevalent at lower ion polishing power densities (energy density per unit duration), irrespective of the duration applied, suggesting that inadequate polishing power density fails to effectively mitigate the transformation. Conversely, unexpectedly, higher power densities also resulted in "No Go" categorisations, revealing that optimal "Go" configurations exist within a specific range of both energy density and duration parameters. Intriguingly, the occurrence of unexpected Co phases, encompassing both ion and mechanical polishing, underscores a cumulative impact of the entire preparation process on the martensitic transformation. Thus, the total Co_{HCP} artefacts observed post-preparation is a collective result of the transformations induced by both mechanical and ion polishing stages, as illustrated in Fig. 10(a).

Moreover, Fig. 10(b) provides schematic depictions of the WC–Co surface anomalies resulting from "No Go" ion polishing steps, offering insights into the challenges and considerations necessary for preserving the pristine Co structure during metallographic preparation.

Relative to WC particles, the Co binder exhibits much faster removal rates and higher plasticity. The "large-ion polishing energy with short-duration" configuration effectively strips the top Co layer, whereas the "large-ion polishing energy with long-duration" also deforms the underlying Co, risking the martensitic Co_{FCC}-Co_{HCP} phase transformation.

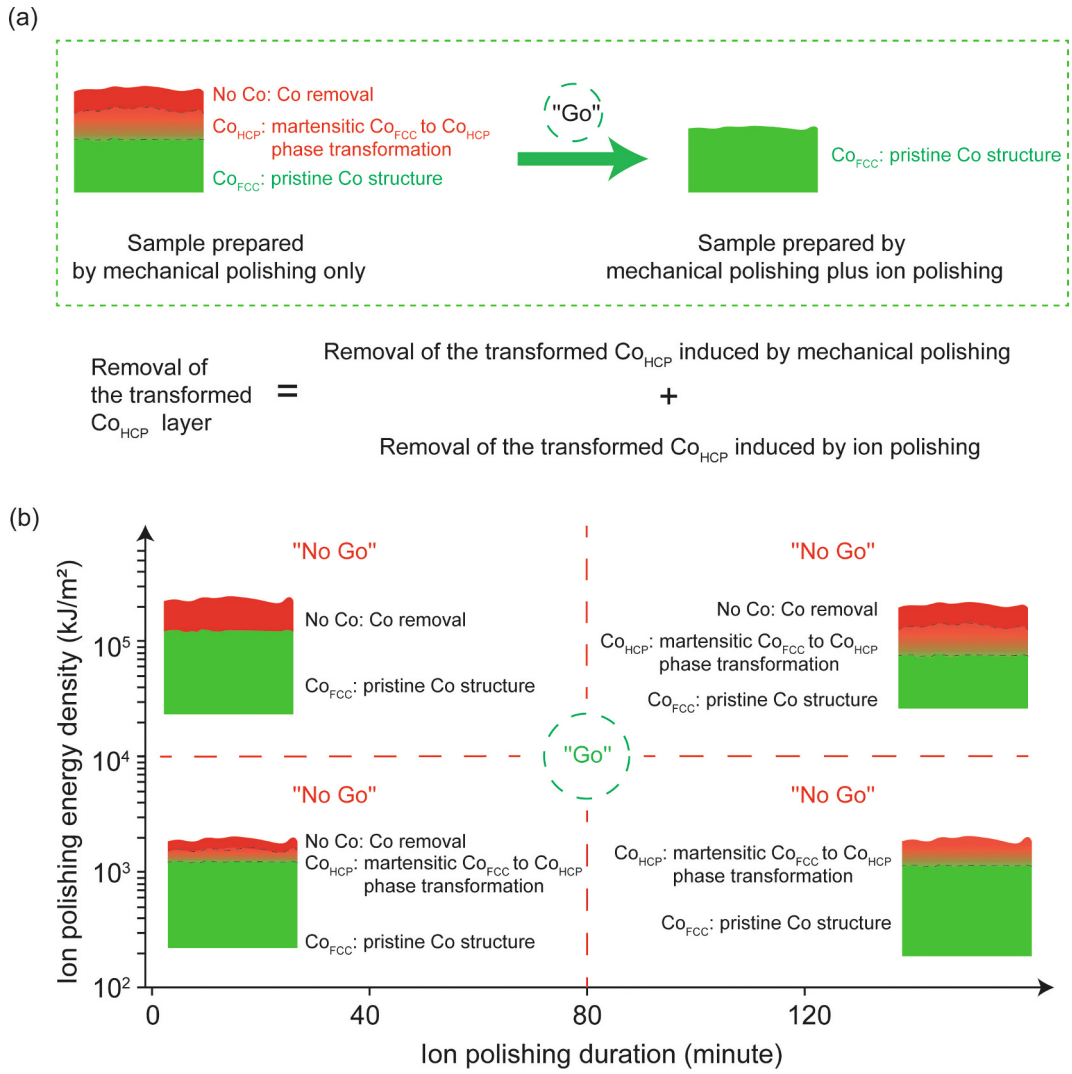

Fig. 10. Overview of Ion Polishing Energy Density Versus Duration on Pristine Co Phase Preservation. (a) Demonstration of the effectiveness of "Go" configurations in removing artefactual Co_{HCP} structures and strategies for preserving the pristine Co phase in fine-grained WC–10Co–1.5Ru–0.6Cr_3C_2 samples. (b) Exploration on the impact of various ion polishing energies and durations on suppressing the martensitic transformation of the pristine Co phase during metallographic preparation. "Go" region indicates configurations that effectively suppress the martensitic Co_{FCC}–Co_{HCP} phase transformation, while "No Go" regions highlight configurations leading to undesirable experimental outcomes, providing critical insights into optimal preparation techniques.

Conversely, "low-ion polishing energy with short-duration" may fail to adequately clear the "mechanically polished" surface, and "low-ion polishing energy with long-duration" gradually deforms the Co, enhancing the risk of martensitic Co_{FCC}-Co_{HCP} phase transformation.

In our study, the optimal "Go" ion polishing configuration falls within an energy density range of ~10.4 to 13.5 MJ/m^2 and a duration of ~80 min, balancing effective removal of deformations and preservation of the pristine Co structure.

5. Conclusions

In this study, we present a detailed comparative analysis aimed at precisely identifying and characterising the pristine Co phase in a series of WC–Co cemented carbides. Advanced multi-scale microscopy and microanalysis, such as XRD, EBSD, TEM, and TKD have been used. By systematically exploring both conventional and advanced techniques, including mechanical polishing and ion polishing, we identified optimal methods that enhance surface quality and enable artefact-free microstructural characterisation. The findings underscore the importance of selecting appropriate preparation workflows, enabling to offer a valuable reference for future studies in structural and property analyses. For plane-polished cross-sections used in (e.g.) EBSD analysis, we find that:

- Mechanical polishing with a hard cloth compared to a soft cloth dramatically reduces the unindexed backscattered diffraction signal from ~23.24 % (soft) to ~13.33 % (hard) (area fraction), enabling a more representative measurement of the phase fractions in WC–Co cemented carbide samples.
- Unfortunately, the hard cloth unequivocally induces the martensitic Co_{FCC}–Co_{HCP} phase transformation under certain circumstances. Therefore, whilst the use of the hard cloth is important to disambiguate the EBSD indexing as described above, it does not suffice as a final polish.
- After the hard cloth polishing, a subsequent Ar^+ ion polishing with ~10 MJ/m^2 for 80 min was found to mitigate artefacts, and eliminate the martensitic Co_{FCC}–Co_{HCP} phase transformation region. We describe the relationship between the ion polishing energy density and duration in terms of suppression of the martensitic Co_{FCC}–Co_{HCP} phase transformation for plane-polished cross-sections.

For thin-sections such as used in (e.g.) TEM analysis, we find that:

- Tripod polishing followed by precision ion polishing with Ar^+ ions effectively reveal the pristine Co structure, without artefacts, and was classified as the preferred method for preparing TEM/TKD samples.
- The application of a Xe^+ focused ion beam was shown to facilitate the martensitic Co_{FCC}–Co_{HCP} phase transformation under both ambient and cryogenic milling conditions, necessitating cautious use of this technology in sample preparation workflows.

CRediT authorship contribution statement

Haoruo Zhou: Writing – review & editing, Writing – original draft, Visualization, Validation, Methodology, Formal analysis, Data curation, Conceptualization. **Hansheng Chen:** Writing – review & editing, Supervision, Methodology, Investigation, Conceptualization. **Christoph Czettl:** Writing – review & editing, Investigation. **Thomas Weirather:** Writing – review & editing, Investigation. **Julia Pachlhofer:** Writing – review & editing, Investigation. **Pauline Mueller:** Writing – review & editing, Investigation. **Tamara Teppernegg:** Writing – review & editing, Investigation. **Ralph Useldinger:** Writing – review & editing. **Sophie Primig:** Writing – review & editing. **Simon P. Ringer:** Writing – review & editing, Supervision, Resources, Project administration, Investigation, Funding acquisition.

Declaration of competing interest

The authors declare that they have no known conflict of interest that could have appeared to influence the work reported in this paper.

Acknowledgement

The authors acknowledge the facilities, the scientific, and technical assistance of the teams at Sydney Microscopy & Microanalysis (SMM) and Sydney Analytical (SA), which are Core Research Facilities at the University of Sydney. SMM is the University of Sydney"s (USYD) node of Microscopy Australia. This work was supported by the Australian Research Council (LP190100850). The authors also acknowledge the contributions of Dr. Xiangyuan Cui, Dr. Hongwei Liu and Dr. Ehsan Farabi for their insightful discussions related to this work, and Dr. Kay Song for assistance with preparation of the manuscript.

Data availability

Data will be made available on request.

References

[1] B. Roebuck, E.A. Almond, Deformation and fracture processes and the physical metallurgy of WC–Co hardmetals, Int. Mater. Rev. 33 (1) (1988) 90–112, https://doi.org/10.1179/imr.1988.33.1.90.
[2] S.-H. Chang, S.-L. Chen, Characterization and properties of sintered WC–co and WC–Ni–Fe hard metal alloys, J. Alloys Compd. 585 (2014) 407–413, https://doi.org/10.1016/j.jallcom.2013.09.188.
[3] J. García, V. Collado Ciprés, A. Blomqvist, B. Kaplan, Cemented carbide microstructures: a review, Int. J. Refract. Met. Hard Mater. 80 (2019) 40–68, https://doi.org/10.1016/j.ijrmhm.2018.12.004.
[4] S. Okamoto, Y. Nakazono, K. Otsuka, Y. Shimoitani, J. Takada, Mechanical properties of WC/co cemented carbide with larger WC grain size, Mater. Charact. 55 (4–5) (2005) 281–287, https://doi.org/10.1016/j.matchar.2005.06.001.
[5] X. Liu, X. Song, H. Wang, X. Liu, F. Tang, H. Lu, Complexions in WC–Co cemented carbides, Acta Mater. 149 (2018) 164–178, https://doi.org/10.1016/j.actamat.2018.02.018.
[6] P.R. Cantwell, M. Tang, S.J. Dillon, J. Luo, G.S. Rohrer, M.P. Harmer, Grain boundary complexions, Acta Mater. 62 (2014) 1–48, https://doi.org/10.1016/j.actamat.2013.07.037.
[7] H.-O. Andrén, Microstructures of cemented carbides, Mater. Des. 22 (6) (2001) 491–498, https://doi.org/10.1016/S0261-3069(01)00006-1.
[8] J.M. Marshall, A. Kusoffsky, Binder phase structure in fine and coarse WC–co hard metals with Cr and V carbide additions, Int. J. Refract. Met. Hard Mater. 40 (2013) 27–35, https://doi.org/10.1016/j.ijrmhm.2013.04.001.
[9] I. Weißensteiner, et al., Deformation-induced phase transformation in a co-Cr-W-Mo alloy studied by high-energy X-ray diffraction during in-situ compression tests, Acta Mater. 164 (2019) 272–282, https://doi.org/10.1016/j.actamat.2018.10.035.
[10] A. Mani, Salinas-Rodriguez, H.F. Lopez, Deformation induced FCC to HCP transformation in a co–27Cr–5Mo–0.05C alloy, Mater. Sci. Eng. A 528 (7–8) (2011) 3037–3043, https://doi.org/10.1016/j.msea.2010.12.024.
[11] B.-S. Lee, Y. Koizumi, H. Matsumoto, A. Chiba, Collective behavior of strain-induced martensitic transformation (SIMT) in biomedical co–Cr–Mo–N alloy polycrystal: an ex-situ electron backscattering diffraction study, Mater. Sci. Eng. A 611 (2014) 263–273, https://doi.org/10.1016/j.msea.2014.05.071.
[12] Y. Koizumi, et al., Strain-induced martensitic transformation near twin boundaries in a biomedical co–Cr–Mo alloy with negative stacking fault energy, Acta Mater. 61 (5) (2013) 1648–1661, https://doi.org/10.1016/j.actamat.2012.11.041.
[13] K.P. Mingard, et al., Comparison of EBSD and conventional methods of grain size measurement of hardmetals, Int. J. Refract. Met. Hard Mater. 27 (2) (2009) 213–223, https://doi.org/10.1016/j.ijrmhm.2008.06.009.
[14] K.P. Mingard, M.G. Gee, EBSD examination of worn WC/co hardmetal surfaces, Wear 263 (1–6) (2007) 643–652, https://doi.org/10.1016/j.wear.2006.11.039.
[15] M. Pourbaix, Atlas of Electrochemical Equilibria in Aqueous Solutions, National Association of Corrosion Engineers (NACE), Housten, 1974.
[16] L. Zhang, Y. Chen, Q. Wan, T. Liu, J. Zhu, W. Tian, Electrochemical corrosion behaviors of straight WC–co alloys: exclusive variation in grain sizes and aggressive media, Int. J. Refract. Met. Hard Mater. 57 (2016) 70–77, https://doi.org/10.1016/j.ijrmhm.2016.02.009.
[17] S. Guo, R. Bao, J. Yang, H. Chen, J. Yi, Effect of Mo and Y 2 O 3 additions on the microstructure and properties of fine WC–Co cemented carbides fabricated by spark plasma sintering, Int. J. Refract. Met. Hard Mater. 69 (2017) 1–10, https://doi.org/10.1016/j.ijrmhm.2017.07.010.
[18] S. Hochstrasser-Kurz, et al., ICP-MS, SKPFM, XPS, and microcapillary investigation of the local corrosion mechanisms of WC–co Hardmetal, J. Electrochem. Soc. 155 (8) (2008) C415, https://doi.org/10.1149/1.2929822.
[19] C.H. Vasel, A.D. Krawitz, E.F. Drake, E.A. Kenik, Binder deformation in WC-(co, Ni) cemented carbide composites, Metall. Trans. A. 16 (12) (1985) 2309–2317, https://doi.org/10.1007/BF02670431.
[20] V.K. Sarin, T. Johannesson, On the deformation of WC–co cemented carbides, Met. Sci. 9 (1) (1975) 472–476, https://doi.org/10.1179/030634575790444531.
[21] M. Rettenmayr, H.E. Exner, W. Mader, Electron microscopy of binder phase deformation in WC–co alloys, Mater. Sci. Technol. 4 (11) (1988) 984–990, https://doi.org/10.1179/mst.1988.4.11.984.
[22] U. Schleinkofer, H.-G. Sockel, K. Gorting, W. Heinrich, Microstructural processes during subcritical crack growth in hard metals and cermets under cyclic loads, Mater. Sci. Eng. A 209 (1–2) (1996) 103–110, https://doi.org/10.1016/0921-5093(95)10098-9.
[23] S. Kursawe, Ph. Pott, H.G. Sockel, W. Heinrich, M. Wolf, On the influence of binder content and binder composition on the mechanical properties of hardmetals, Int. J. Refract. Met. Hard Mater. 19 (4–6) (2001) 335–340, https://doi.org/10.1016/S0263-4368(01)00026-9.
[24] J. Yang, J.J. Roa, M. Schwind, M. Odén, M.P. Johansson-Jõesaar, L. Llanes, Grinding-induced metallurgical alterations in the binder phase of WC–Co cemented carbides, Mater. Charact. 134 (2017) 302–310, https://doi.org/10.1016/j.matchar.2017.11.004.
[25] K.P. Mingard, B. Roebuck, J. Marshall, G. Sweetman, Some aspects of the structure of cobalt and nickel binder phases in hardmetals, Acta Mater. 59 (6) (2011) 2277–2290, https://doi.org/10.1016/j.actamat.2010.12.004.
[26] I. Borgh, et al., On the three-dimensional structure of WC grains in cemented carbides, Acta Mater. 61 (13) (2013) 4726–4733, https://doi.org/10.1016/j.actamat.2013.05.008.
[27] K.P. Mingard, H.G. Jones, M.G. Gee, B. Roebuck, J.W. Nunn, In situ observation of crack growth in a WC–Co hardmetal and characterisation of crack growth morphologies by EBSD, Int. J. Refract. Met. Hard Mater. 36 (2013) 136–142, https://doi.org/10.1016/j.ijrmhm.2012.08.006.
[28] C. Xiang, et al., Atomistic observation of in situ fractured surfaces at a V-doped WCCo interface, J. Mater. Sci. Technol. 110 (2022) 103–108.
[29] C. Yang *et al.*, "Interfacial superstructures and chemical bonding transitions at metal-ceramic interfaces," Sci. Adv., vol. 7, no. 11, p. eabf6667, doi: https://doi.org/10.1126/sciadv.abf6667.
[30] B. Winiarski, A. Gholinia, K. Mingard, M. Gee, G.E. Thompson, P.J. Withers, Broad ion beam serial section tomography, Ultramicroscopy 172 (2017) 52–64, https://doi.org/10.1016/j.ultramic.2016.10.014.
[31] T.L. Burnett, et al., Large volume serial section tomography by Xe plasma FIB dual beam microscopy, Ultramicroscopy 161 (2016) 119–129, https://doi.org/10.1016/j.ultramic.2015.11.001.
[32] J.-C. Zhao, M.R. Notis, Kinetics of the fcc to hcp phase transformation and the formation of martensite in pure cobalt, Scr. Metall. Mater. 32 (10) (1995) 1671–1676, https://doi.org/10.1016/0956-716X(95)00253-R.
[33] M. Eizadjou, H. Chen, C. Czettl, J. Pachlhofer, S. Primig, S.P. Ringer, An observation of the binder microstructure in WC-(co+Ru) cemented carbides using transmission Kikuchi diffraction, Scr. Mater. 183 (2020) 55–60, https://doi.org/10.1016/j.scriptamat.2020.03.010.
[34] D. Wang, Y. Huang, B. Liu, L. Zhu, J. Lam, Z. Mai, A developed wedge fixtures assisted high precision TEM samples pre-thinning method: towards the batch lamella preparation, AIP Adv. 7 (4) (2017) 045207, https://doi.org/10.1063/1.4980022.
[35] J.H. Dycus, J.M. Lebeau, A reliable approach to prepare brittle semiconducting materials for cross-sectional transmission electron microscopy, J. Microsc. 268 (3) (2017) 225–229, https://doi.org/10.1111/jmi.12601.

[36] Á. Barna, B. Pécz, M. Menyhard, TEM sample preparation by ion milling/amorphization, Micron 30 (3) (1999) 267–276, https://doi.org/10.1016/S0968-4328(99)00011-6.
[37] D.K. Schreiber, D.E. Perea, J.V. Ryan, J.E. Evans, J.D. Vienna, A method for site-specific and cryogenic specimen fabrication of liquid/solid interfaces for atom probe tomography, Ultramicroscopy 194 (2018) 89–99, https://doi.org/10.1016/j.ultramic.2018.07.010.
[38] J. Perret, et al., EBSD, SEM and FIB characterisation of subsurface deformation during tribocorrosion of stainless steel in sulphuric acid, Wear 269 (5–6) (2010) 383–393, https://doi.org/10.1016/j.wear.2010.04.023.
[39] K. Thompson, D. Lawrence, D.J. Larson, J.D. Olson, T.F. Kelly, B. Gorman, In situ site-specific specimen preparation for atom probe tomography, Ultramicroscopy 107 (2–3) (2007) 131–139, https://doi.org/10.1016/j.ultramic.2006.06.008.
[40] J.H. Yang, C.M. Wayman, On secondary variants formed at intersections of ϵ martensite variants, Acta Metall. Mater. 40 (8) (1992) 2011–2023, https://doi.org/10.1016/0956-7151(92)90187-J.